AAS 07-062

A new Concept for a Low-Cost Earth Sensor: Imaging Oxygen Airglow with Arrays of Single Photon Detectors

N. Scheidegger, R. Krpoun, H. Shea, C. Niclass and E. Charbon
Ecole Polytechnique Fédérale de Lausanne (EPFL)
Lausanne, Switzerland

30th ANNUAL AAS GUIDANCE AND CONTROL CONFERENCE

February 3-7, 2007
Breckenridge, Colorado

Sponsored by
Rocky Mountain Section

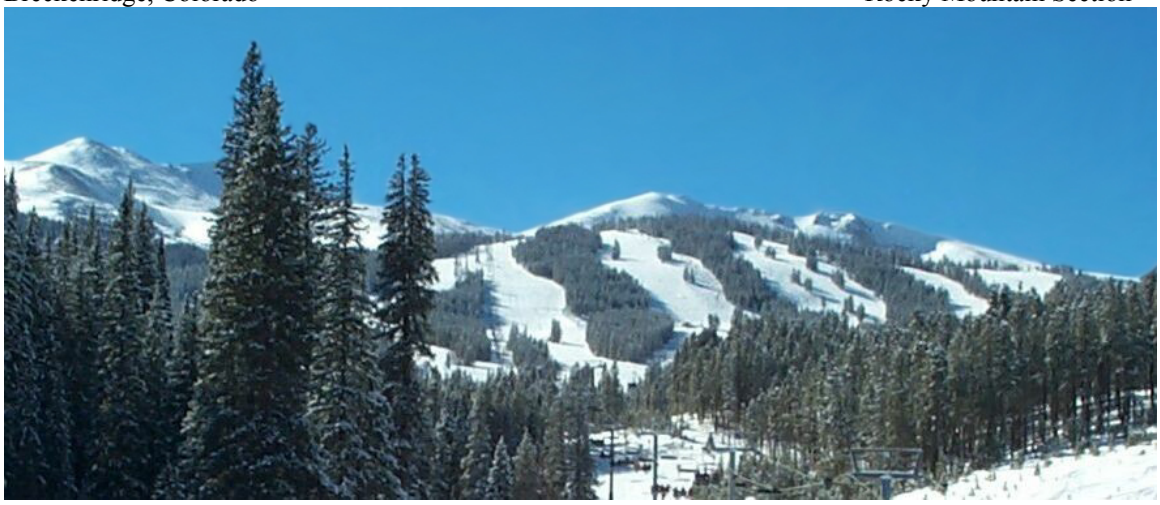

AAS Publications Office, P.O. Box 28130 - San Diego, California 92198

A NEW CONCEPT FOR A LOW-COST EARTH SENSOR: IMAGING OXYGEN AIRGLOW WITH ARRAYS OF SINGLE PHOTON DETECTORS

N. Scheidegger, R. Krpoun and H. Shea*

C. Niclass and E. Charbon†

This paper presents a novel concept for a compact low-cost Earth sensor based on imaging atmospheric oxygen emission at 762 nm using arrays of single photon avalanche diodes (SPADs). In both nighttime and daytime there is continuous emission at 762 nm due to oxygen recombination. The SPADs high sensitivity enables the ES to operate at night and day, over a wide temperature range, with a very compact optical system (e.g. aperture of 10 mm, focal length of 14 mm) and no scanning elements. A modular and low-cost instrument design is described, which uses the same wavelength band, the same detector technology, the same optics, the same power and data interfaces and similar algorithms for LEO and GEO applications. Using the visible band rather than the LWIR band offers several advantages including much lower cost detectors, no need for cooling, a more relaxed thermal design, simpler optics, higher sensitivity and hence low cost.

1. INTRODUCTION

Available Earth Sensors (ES) are based on the measurement of Earth's infrared radiation (typically between 14 and 16 μm) to determine the vector to the Earth's centre. Standard designs use bolometers, thermopiles or semiconductor-based detectors, often combined with scanning mirrors to provide excellent accuracies (tens of milli-degrees) over a large field of view. However, these designs are heavy, large, require cooling or temperature stabilization and are power hungry. In addition, the sensor concept for a LEO or GEO Earth Sensor differs significantly, typically requiring two different designs and qualification procedures and therefore increasing the ES cost.

* Microsystems for Space Technologies Laboratory EPFL, Ecole Polytechnique Fédérale de Lausanne, CH-1015 Lausanne, Switzerland, Contact: herbert.shea@epfl.ch +41 32 720 5584

† Quantum Architecture Group EPFL, Ecole Polytechnique Fédérale de Lausanne, CH-1015 Lausanne, Switzerland

The availability of low cost Earth Sensors would allow ES to be used in new scenarios and to improve system reliability by providing a low-cost back-up sensor. Examples of applications where neither milli-degree accuracy nor operation at high angular rates are required, but where low-cost is essential and lower (about 1° to 5°) accuracy is acceptable, include:

- LEO Initial Acquisition and Safe Mode Sensor
- GEO and LEO Back-up sensor for Earth-pointing safe modes
- GEO Earth Presence Anomaly Sensor

Approximate requirements for such an ES are an accuracy of 0.6° for GEO and 5° for LEO, mass of under 750g, and power consumption of less than 5 W. Scanning optics and shutters must be avoided for reliability considerations, and the ES must be capable of staring at the sun for over 10 hours with no damage. In order to reduce cost, non-traditional approaches have to be taken with respect to the wavelength band used for observation, the detector technology, and the algorithms.

Two major technological innovation areas are enabling new lower cost architectures for Earth Sensors that could allow for dramatically lower power consumption, a smaller mass and volume, and can allow for similar qualification process for LEO and GEO orbits.

The first area with major progress is the field of uncooled detectors for the infrared observation band. Bolometer arrays fabricated using MEMS technologies are becoming available with high enough performance for ES applications. The emergence of this uncooled detector technology encourages the continued use of the proven far-infrared emission bands and allows the reuse of established algorithms.

The other area of rapid technological progress is the increased sensitivity and performance of Charge Coupled Devices (CCDs) and especially new CMOS–based detector technologies such as single-photon avalanche diode (SPAD) arrays. These techniques are highly sensitive in the visible bands and near-IR (0.4 μm to 1 μm wavelength) and very mature in the commercial market.

We describe in this paper a concept for a low cost Earth Sensors based on imaging atmospheric oxygen emission at 762 nm using arrays of single photon avalanche diodes (SPADs). The second section summarizes the available data on airglow emissions. In the third section the Earth appearance at 762 nm is presented. The principle of operation and architecture of the Single Photon Avalanche Diodes (SPADS) arrays for the ES are presented in fourth section, whereas the oxygen airglow-based ES concept and its predicted performance is described in fifth section.

2. AIRGLOW EMISSIONS

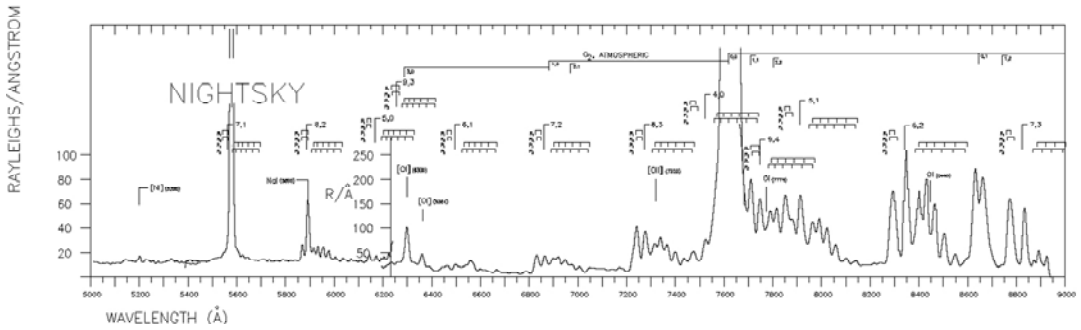

Figure 1: Limb measure of nightglow.[1]

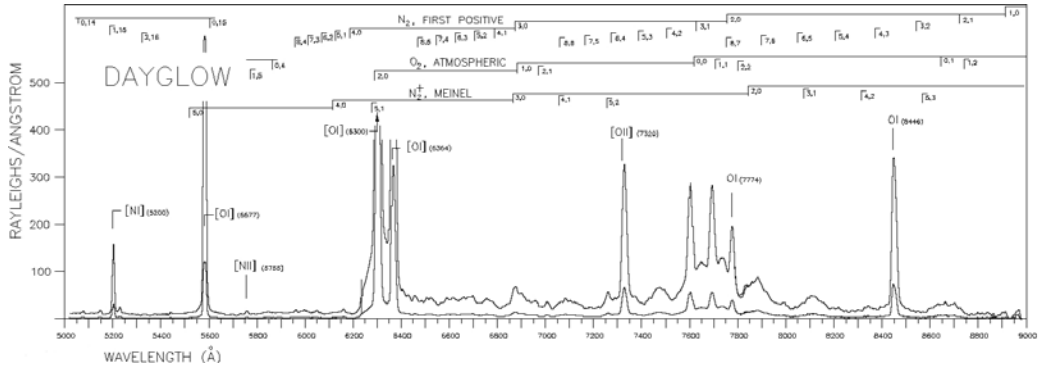

Figure 2: Limb measure of dayglow.[1]

Atmospheric emissions in the wavelength band from 500 to 900 nm can be classified as: nightglow, dayglow and aurora. Nightglow and dayglow are the only potential candidates for detection by an Earth Sensor because of their permanence. Figure 1 and 2 show the airglow spectra between 500 and 900 nm. Emission is measured in Rayleighs [R]. The most prominent feature, visible from Earth, is the atomic oxygen $O(^1S)$ green line at 557.7 nm, whereas the strongest airglow band, only visible from space, is the O_2(0-0) A-band at 762 nm. These two oxygen emissions could be used as basis for the Earth Sensor. For both wavelengths, aurora and dayglow originate with direct photodissociation, photo-excitation and excitation by fast electrons or ion recombination. The origin of the nightglow is oxygen atom recombination, where the oxygen atoms are created in the daytime by solar photodissociation of O_2. [1]

A number of studies exist on the temporal and latitudinal variability in the oxygen emissions in the 50–120 km region of the mesosphere and lower thermosphere. The main data on airglow emission were obtained with the Wind Imaging Interferometer (WINDII) and the High Resolution Doppler Imager (HRDI) on the UARS satellite and the Optical Spectrograph and Infrared Imager System (OSIRIS) on the ODIN satellite. They provide a wide database on the airglow emission rates of the 557.7 nm line and the 762 nm band for different altitudes, local times and latitudes.[3] The oxygen airglow emission rate is modulated by atmospheric tides and by semi-annual, annual and longer-term variations as for example the solar cycle. Figure 3 describes a typical tidal variation of the nightglow volume emission, whereas Figure 4 shows the airglow layer.

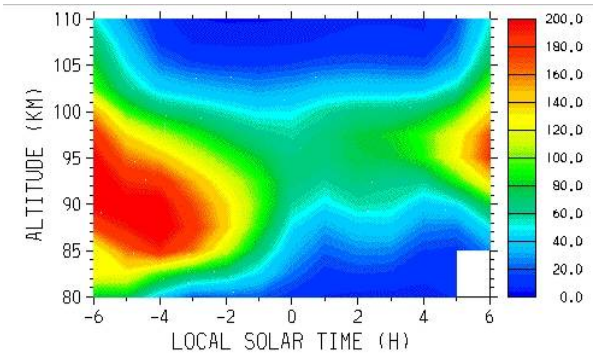

Figure 3: Tidal variation of nightglow emission of the O(^{1}S) line at 557.7 nm [photons/cm^3/s].[4]

Figure 4: Airglow layer, aurora borealis and city lights (picture taken by STS-108).

The 762 nm O_2(0-0) A-Band molecular oxygen band emits the strongest airglow, with intensities varying from 2 kR to 1.5 MR at zenith and 20 kR and 18 MR at limb (see Table 1). Limb emissions are 10 to 15 times stronger than zenith emissions due to the fact that the emissions brightness represents an integrated volume emission rate along the line of sight. Thus, images of the airglow will be characterized by a continuously increasing emission intensity towards the limb, a peak brightness at an altitude of 60 km during day and 95 km at night, and a sudden drop of the emissions intensity when reaching the maximum altitude of airglow emission around 120 km. The emission of the O_2(0-0) A-Band is not visible form the ground because of the deep absorption by the dense lower atmospheric O_2 – layer at an altitude of 60 km. This is a significant advantage for space based observations since this layer will act as a filter for the rescattered emission by the Earth due to sun- or moonlight. Thus, the main sources of perturbation in the airglow are auroras which emit weakly at 762 nm. Measurements of the 762 nm O_2(0-0) A-Band can be used to get information about the ozone profile, the temperature climatology for mesopause region or atmospheric winds.

Table 1

AIRGLOW OF THE O_2(0-0) A-BAND AT 762 NM [5,6]

	At zenith (R)	At limb (R)
At night	2 k – 10 k	20 k – 150 k
At day	200 k – 1.5 M	4 M – 18 M
Aurora perturbations	200 – 7 k	100 – 3.5 k

The O(^{1}S) green line emission at 557.7 nm is the most extensively studied of the emissions discussed in this paper. The main interest of the emission at 557.7 nm is its visibility from the ground and the fact that it is closely related to the concentration of atomic oxygen density. Hence, the green line provides information on the ozone or atmospheric winds, similar to the emissions at 762 nm. However, the emissions at 557.7 nm are significantly weaker than those at 762 nm. Intensities vary between 40 R and 12 kR for zenith observations, respectively 450 R and 150 kR at limb. Furthermore, auroras have strong emissions at 557.7 nm and might seriously perturb the airglow measurements (see Table 2).

Table 2

AIRGLOW OF THE O(^{1}S) GREEN LINE AT 557.7 NM [5,6]

	At zenith (R)	At limb (R)
At night	40 – 400	450 – 4 k
At day	1.2 k – 12 k	12 k – 150 k
Aurora perturbations	1 k – 1 M	0.5 k – 500 k

For space observations, the emission of the O_2(0-0) A-Band at 762 nm has several advantages compared to the 557.7 nm line. These emissions are stronger and less perturbed by background radiation or aurora effects. They provide a more constant and strong light source and hence the better basis for an Earth Sensor.

3. EARTH APPEARANCE MODEL AT 762 NM

In order to determine the requirements on the SPAD detector array and the optical system an Earth Appearance Model has been developed. This model simulates the appearance of the Earth at 762 nm as seen from a satellite in a GEO and includes

- The minimum, maximum and mean airglow emissions at 762 nm
- Variations in airglow intensity depending on the local solar time
- Aurora effects around the poles
- Perturbations due to the moon (direct reflection of the sunlight)

The Earth Appearance Model provides the mean, min and maximum expected photon flux on a pixel of the detector depending on the optical aperture of the instrument and the local solar time at zenith. It is based on the observations carried out by the High Resolution Doppler Imager (HRDI) instrument aboard the Upper Atmosphere Research Satellite (UARS). This instrument observed the emission of molecular oxygen above the limb of the Earth in order to deduce from it information about atmospheric winds, temperature and ozone. Measurements of oxygen volume emission rates have been taken from 1991 to 1999 and cover almost all daylight and nocturnal time.

An analysis of the UARS data allowed identifying the main parameters for airglow emission: altitude, local solar time, latitude, seasonal variations and long-term variations. It is important to note that there are no significant variations depending on longitude. Since the Earth Appearance Model is used to determine the requirements on the SPAD array and the optical system, it shall simulate the image of the Earth at 762 nm in the worst conditions for the Earth Sensor, hence when the largest variations in emission intensity are expected. Since the airglow has a strong dependence on the solar illumination, the biggest intensity gradient will be observed during winter and summer. Figure 5 shows the volume emission rate of the O_2(0-0) A-Band at different altitudes depending on local solar time and latitude. These values have been extracted from the HRDI observations made in winter from 1991 to 1999.[*]

[*] It is important to note that there is always airglow, even if it might not be visible in Figure 5.

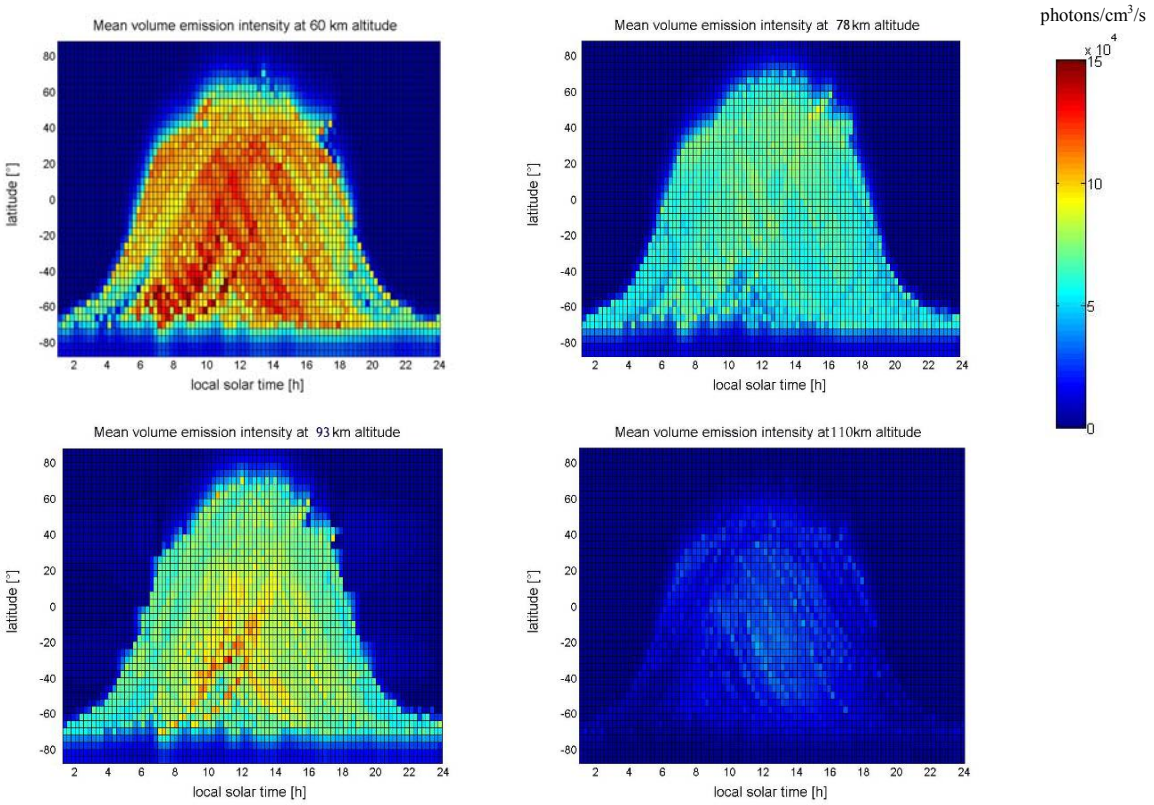

Figure 5: Volume emission rate of the O2 (0-0) A-Band at different altitudes depending on local solar time and latitude. [based on data from UARS]

To simulate the image of the Earth as seen from a satellite, a 3-D space relating each point to a certain local solar time, altitude and latitude has been built. The image can be calculated by integrating the volume emission rate along the line of sight of each point of the image. The effective photon flux on a single pixel of the detector can be calculated with the Eq. (1),[7]

$$\Phi_{pixel} = \Phi_{airglow} \frac{1}{4\pi} 10^4 \cdot A_D \cdot \omega \qquad [photons/s^{-1}] \qquad (1)$$

where A_D is the aperture of the telescope [m^2] and ω is the solid acceptance angle [sr]. As shown on the images here after, there will always be a signal emitted at the limb which is usable to calculate the Earth vector.

Mean airglow emission at 24:00 SLT Mean airglow emission at 06:00 SLT Mean airglow emission at 12:00 SLT

Figure 6: Signal emitted by the airglow as seen from a GEO for different local solar times at zenith.

The Earth Appearance Model was extended to simulate the airglow emissions as seen with the SPAD array by introducing a *dark count rate* (DCR, a measure of intrinsic noise), a lower pixel resolution corresponding to the planned 128x128 array, and a varying optical aperture. It allows analyzing the impact of these parameters on the airglow observations and helps design and test the algorithms to determine the Earth center. The analysis based on the Earth Appearance Model will provide requirements on the SPAD array (pitch size and read-out method) and on the optical system (optical aperture and focal length). Current baseline values can be found in the fifth section.

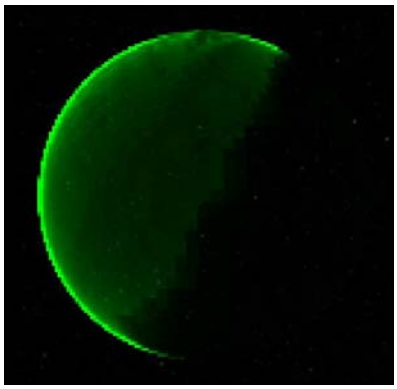

Figure 7: Simulation of the airglow measurement with the SPAD array assuming a DCR of 30 Hz.

4. SINGLE PHOTON AVALANCHE DIODES

Solid-state implementations of single photon counters have existed for many decades. However, the first single photon avalanche diode (SPAD) fully integrated in CMOS was successfully designed only in 2003.[8] The device comprises a pn junction and a structure to prevent early discharge at the corners of the junction. This structure is usually a lightly doped p or n tub surrounding the junction. Ideally, the multiplication region is circular, to prevent edge non-uniformities and zones of high electric field. Figure 8 shows the cross-section of a SPAD implemented in CMOS technology.

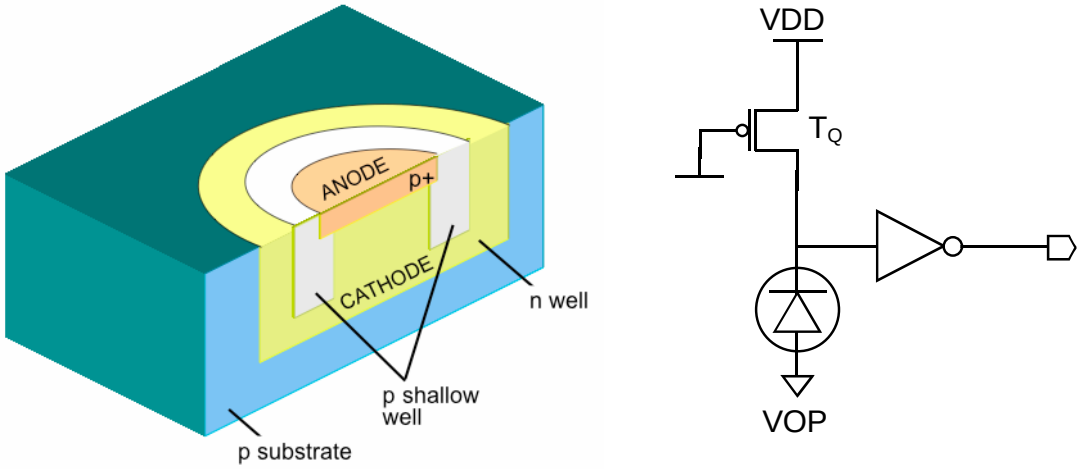

Figure 8: Cross-section of a typical SPAD implemented in CMOS technology (left); schematic (right).

If the pn junction is biased *above* breakdown, its optical gain becomes virtually infinite, enabling detection of single photons. When a photon impinging the surface of the semiconductor is absorbed, it may create an electron-hole pair in the multiplication region. The carriers by impact ionization may trigger an avalanche that needs to be quenched.

There exist several techniques to quench an avalanche.[9] In this design a passive quenching is adopted, which is achieved by placing a resistor in series to the diode. When the avalanche current passes through the resistor, it generates a voltage drop across the diode, thus bringing its bias below breakdown and hence stopping the avalanche. After a recharge time, limited by the RC constant of the quenching resistor and the sum of all parasitic capacitances at the cathode, the SPAD is ready to the next detection. This time is known as *dead time* and limits the maximum photon rate that can be detected before reaching saturation. In the current designs the dead time is typically about 40-60ns. Figure 8 shows a CMOS implementation of the SPAD, where the anode is biased at a negative voltage VOP and the avalanche pulse is sensed at the cathode by a comparator or a simple inverter and regenerated by a buffer to drive the necessary load. VOP satisfies the equation $|VOP| + VDD = V_{bd} + V_e$, where VDD, V_{bd}, V_e, are supply, breakdown, and excess bias voltage, respectively. The overall probability that a photon is detected is known as *photon detection probability* (PDP). The PDP has usually a maximum in the central visible range and may reach up to 40-60%.

The noise performance of SPADs is generally characterized in terms of the average rate spurious pulses not due to photons. This rate, known as *dark count rate* (DCR), is determined by thermal and tunneling generation effects. DCR is a function of technology, anode geometry, and temperature, and may vary from a few hertz to a few kilohertz. The dynamic range of SPADs is determined by DCR from below and by saturation from above. Saturation, in turn, is limited by PDP and dead time.

Figure 9 shows the responsivity of a SPAD for a given wavelength and temperature. The dynamic range in this case is 120dB.

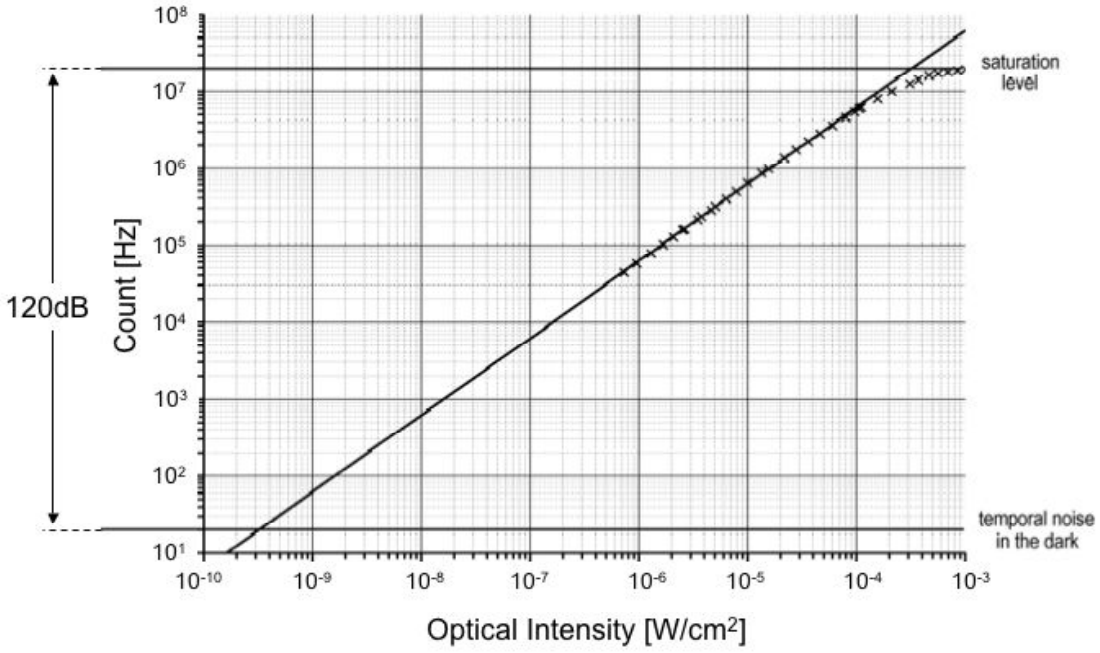

Figure 9: Dynamic range of SPADs for an exposure time of 1s. The measurement was performed at room temperature.

4.1. CMOS SPAD Arrays

Since the introduction of SPADs integrated in CMOS technology, a flurry of activity has lead to the design and demonstration of increasingly larger arrays where every pixel could achieve high timing accuracy, sensitivity, and dynamic range.[10,11,12,13,14] To our knowledge, the largest fully integrated SPAD array has been built by EPFL's Quantum Architecture Group and it is working on even larger arrays.[15] In addition, new application fields of SPAD arrays have been demonstrated, from 3D vision[10,11,16] to two-photon fluorescence lifetime imaging microscopy (FLIM)[17], from low-light-level to ultra-high speed imaging[14], from fluorescence correlation microscopy (FCS)[18] to chip diagnostics.[19]

The fundamental problem of SPAD arrays is the readout, since SPADs are dynamical detectors. The dynamical behavior of SPADs relates to the fact that they generate a logic "1" when a photon is detected. They remain at logic "0" when no photons impinge the surface of detection. Thus, analog readout techniques perfected for CCDs and CMOS APS architectures cannot be used in SPAD imagers. High timing-resolution applications, such as those advocated in (Ref. 20), may take advantage of creative readout solutions[12,21] at a cost of more silicon real estate. However, when power dissipation and area are major constraints, trade-offs must be done. The simplest solution is a sequential readout method.[14] However, light exposure needs be reduced, thus giving up the sensitivity advantages. An alternative is the use of event-driven readout methods, where sensor columns are accessed by each pixel as a bus in time-division multiple access (TDMA).[12,15] A photomicrograph of the chip proposed in (Ref. 15) is shown in Figure 10.

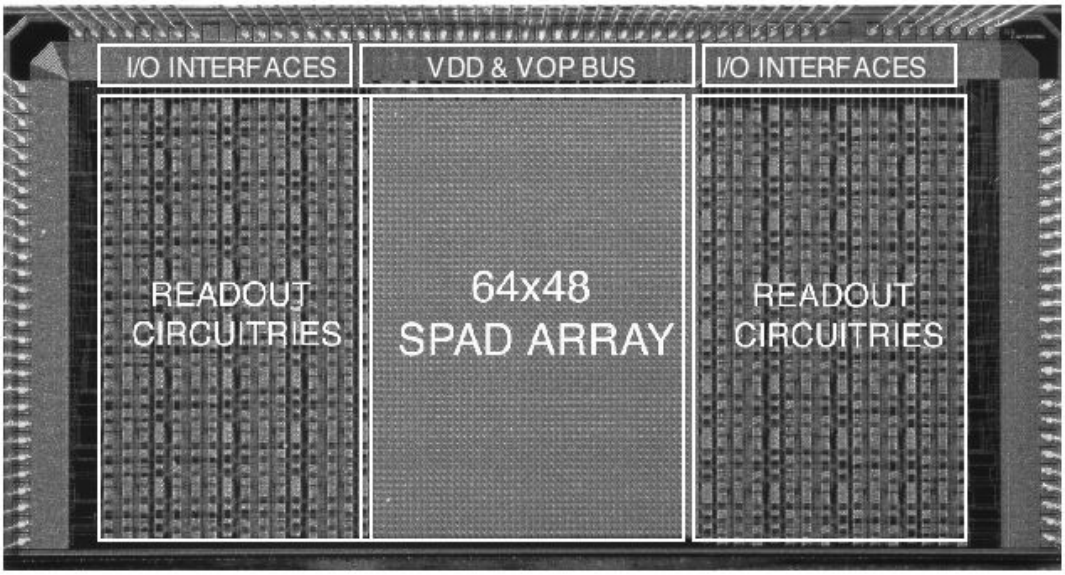

Figure 10: A 64x48 SPAD array with event-driven readout .[15]

To achieve further pitch reduction at little cost of dynamic range and power dissipation, novel architectures based on single bit counting are emerging.[21] This trend is expected to accelerate thanks to more aggressive designs and the use of advanced deep sub-micron technologies. An example of one such readout design is a 128x2 SPAD array sensor for fast timing accurate detection and single bit counting proposed in (Ref. 21). The chip was fabricated in 0.35μm CMOS technology and it exhibits a DCR of 750Hz

and a PDP in excess of 40% at room temperature and an excess bias of 4V. PDP can be traded for a better DCR performance by acting upon the excess bias. This is a technique that can be used on-line or off-line, depending upon the application. Table 3 shows a list of parameters and their typical values as an illustration for a number of SPAD implementations. With the introduction of SPADs fabricated in new processes, significant performance variations may exist.

Table 3

TYPICAL OVERALL PERFORMANCE OF SPAD IMAGERS

Measurement	Min	Typ	Max	Unit
Timing resolution	38	80	145	Ps
DCR (averaged over all pixels)	5		750	Hz
Pixel pitch		45		µm
Fill-factor	1	9		%
V_{OP}	-25		-10	V
V_{DD}	2		5	V
PDP @ 550 nm	26		41	%
EM spectrum (PDP > 1%)	380		900	Nm
Supply current		1	100	mA

5. EARTH SENSOR INSTRUMENT DESIGN

5.1. Conceptual Design

The angular size of the Earth differs significantly if it is seen from a LEO (100 ° to 160 °, see Figure 11) or a GEO, where the Earth's angular size is around 17 °. This difference has an important impact on the conceptual design of the sensor.

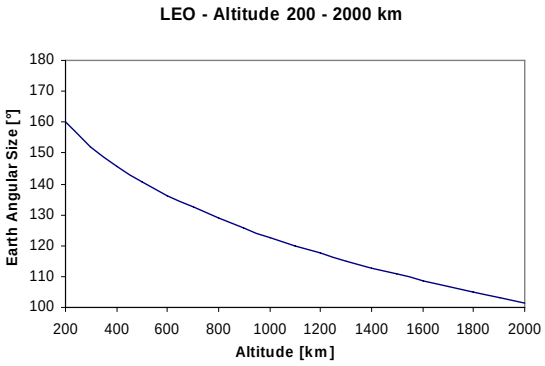

Figure 11: Angular size of the Earth as seen from a LEO.

In this paper a modular and low-cost instrument design is presented, which uses the same wavelength band, the same detector technology, the same optics, the same power and data interfaces and similar algorithms for both orbit classes. However, the optical geometry will be different for an instrument used in a GEO or in a LEO. Whereas

a “single-tube” design covering a FOV of 20° is best suited for GEO (Figure 12.B.), a “triple-tube” concept will be used for LEO in order to provide the required FOV of 180 ° (Figure 12.A.). For both geometries, the volume of the instrument will be minimized, its mass will not exceed 750g and the power consumption will be less than 5 W. The goal is to design the instrument as simple and as compact as possible.

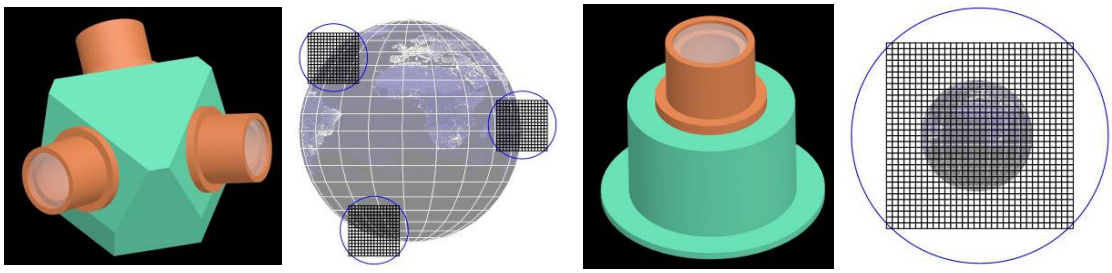

A. LEO **B. GEO**

Figure 12: Possible Earth Sensor configurations and geometries. The dark blue circles mark the telescopes FOV, whereas the black arrays indicate the view of the active sensor elements. A. LEO case at 2’000 km altitude: Three telescopes each with a sensor array and a 20° FOV are used. B. GEO case at 36’000 km altitude: One telescope only, with a FOV of 20° and one detector array.

Note that it is not necessary to have the detector cover the full FOV to accurately determine the Earth vector. Since the Earth is a sphere, the acquisition of two points of the limb is theoretically sufficient to determine the Earth’s center. Nevertheless, further points will be measured in order to improve the reliability of the data and provide redundancy.

5.2. Mechanical Design

The baseline instrument design consists of an optical system, a detector and an electronic circuit. The optical system includes a baffle, a tube, a narrow-band filter centered at 762 nm, focusing optics with a 20° FOV and a micro-lens array bonded to the SPAD detector array in order to increase its fill-factor.

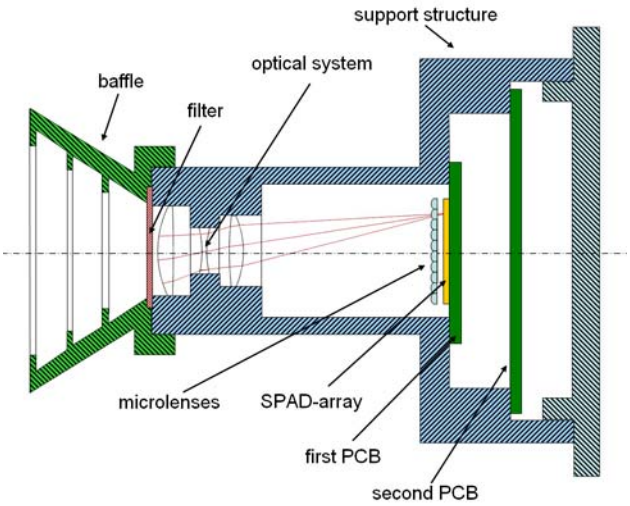

Figure 13: Mechanical design of the ES for GEO applications.

The detector is a SPAD-array with 128 pixels x 128 pixels with a pixel pitch of 60 μm. The active area of the SPAD sensor is 7.68x7.68 mm^2. The optical system and the detector provide a FOV_{pixel} of 0.16 ° per pixel and a total FOV of 20°. An electronic circuit drives the detector, processes the image data to determine the Earth vector and provides the required voltage and current supply.

5.3. Optical Design

In view of the performance goals and cost drivers, the resolution for a system of this type is lower than for a photographic system. The detector and the optical system have to provide a total FOV of 20° and a sufficient resolution to guarantee the targeted X,Y output accuracy of 0.6 ° for a GEO. No chromatic correction of the imaging optics is required since only one wavelength will be observed. Special attention has to be paid to achieve low distortion; an upper limit of 0.1% of allowable distortion is assumed. The primary candidate optical design is a standard triplet lens (Cooke triplet), which has enough degrees of freedom to design an anastigmatic lens.

The most critical component of the optical system is the narrow bandpass filters used for background light suppression. The cut-on and cut-off edges of these elements are kept usually rather steep to achieve an optimum performance. A shift of these edges throughout the lifetime of the system could lead to a dramatic performance loss if the filter bandwidth is not properly dimensioned. The main effects to be taken into account for this dimensioning are aging effects and temperature effects.

Exposure of a film to atmospheric conditions, usually results in a shift of the film characteristic to longer wavelengths. If the filter has been stabilized in atmospheric conditions, it has to be assumed that it will exhibit a spectral shift of -1 nm being exposed to the vacuum in space. In order to cope with the shift towards the blue region and not to cut the used bandwidth channel the filter has to be by +1nm wider at its long wavelength edge. The gradual stabilization of a coating as it reaches equilibrium is referred to as "aging".

The second effect to be considered for the dimensioning of the bandpass filters is the temperature drift; in general, for small temperature changes, the principle effect is a simple shift towards longer wavelengths with increasing temperature. For the materials commonly used in the visible region of the spectrum, the shift is in the order of 0.003% per °C, while for infrared filters it can be greater, and a useful figure is 0.005% per °C.[22]

The filter wavelength and bandwidth is determined by the airglow sources. The large (20°) FOV imposes limits on minimum achievable bandwidth, since most filters are specified for light normal to the plane of the filter. Based on available limb nightglow data, a 5 nm filter bandwidth should be sufficient to ensure that most of the 762 nm band is captured. Thermal consideration will then drive the choice of the effective bandwidth, filter type, and well as double or triple stage filters to eliminate IR and UV light that may pass through a high performance interference filter and degrade the detector or the optics, or even the filter itself.

5.4. Electrical Design

The electronic circuit will include a first PCB with the SPAD detector array and a microcontroller to run the SPADs, and a second PCB with an ASIC for image processing, interfacing and voltage regulators to provide the 3.3 V and 15 V required to operate the SPAD-array.

5.5. Algorithms

The calculations used to determine the Earth's vector should be as simple as possible, but still reliable and robust. As a first iteration, we propose a simple algorithm based on the following concept: Airglow emissions occur in the whole Earth's atmosphere with a maximum at limb. Thus, depending on the way of imaging the airglow, a completely or partially filled circle will be visible on the detector. The algorithm has to find this circle and determine its center. Since the satellite altitude is known, the theoretical radius of the circle on the image is known. This information can be used to cross check the sanity of the sensor.

As mentioned before, there are two options to image the airglow: one is based on saturation of the pixels where airglow emissions occur, the other is working with no or with only limited saturation (Figure 14).*

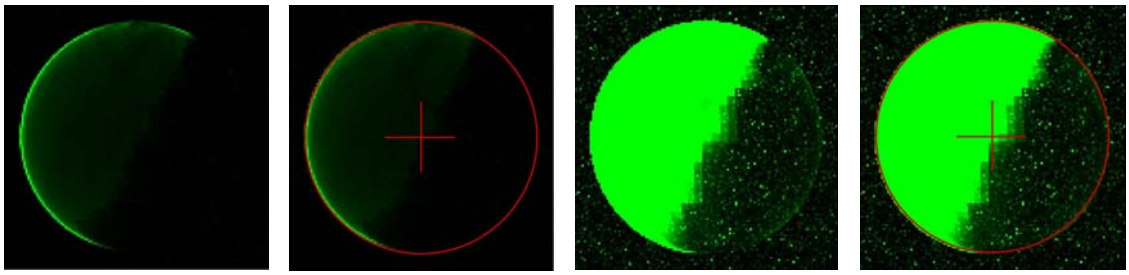

A. (operation without saturation) **B.** (operation in saturation)

Figure 14: A left. Simulated image of the airglow at 06:00 LST assuming a sufficient dynamic range to avoid saturation. A right. The Earth vector is calculated by finding the best correlation between the theoretical circumference of the airglow and the measured maximum emission circle. B left. Simulated image of the airglow at 06:00 LST assuming that the detector saturates under daytime conditions. B right. The Earth vector is calculated by finding the best correlation between the theoretical circumference of the airglow and the measured limb of the Earth.

An algorithm working on saturation is simpler and is insensitive to perturbations due to background radiation, aurora effects or other variations in airglow intensity. The control of the detector is simpler since the read-out frequency is lower. However, the edge detection is less precise and might reduce the accuracy of the Earth vector calculations.

If no saturation is tolerated, the accuracy of the Earth Sensor could be improved by increasing the precision of the Earth limb detection. However, some pre-processing like detection of variations in intensities or local maxima might be required to improve the robustness of the algorithm. Special attention has to be paid on the effect of the zone

* Both simulations include a mean DCR of 30 Hz.

around solar terminator, the moon and the sun. The algorithm has to be able to calculate the Earth vector even if it is perturbed by these phenomena.

In both cases the reliability of this method is higher for an observation from GEO than from LEO, since a larger part of the circumference of the Earth will be imaged on the detector. Thus, the circle can be more accurately fitted. For an image of the airglow taken from LEO only smaller segments of the circle will be visible. Furthermore, the LEO algorithm must determine the Earth vector even if one telescope does not give useful information (because it points at the sun for example).

5.6. Expected performance

The performance of the instrument depends on the aperture of the optical system, the integration time (and hence the refresh rate) of the measurements, the design of the SPAD-array and its read-out method, the way of imaging the airglow (with saturation or not) and the algorithm used to calculate the Earth vector. All these parameters are strongly interconnected: The algorithm determines the way of imaging the airglow and hence the read-out method of the detector and the maximum accepted photon flux before saturation. The aperture size and the integration time affect the minimum photon flux on the detector and thus the Signal-To-Noise-Ratio. Figure 15 shows the mean incident photon flux onto a pixel of the detector for limb measurements at night, depending on the telescope aperture and the satellite altitude.

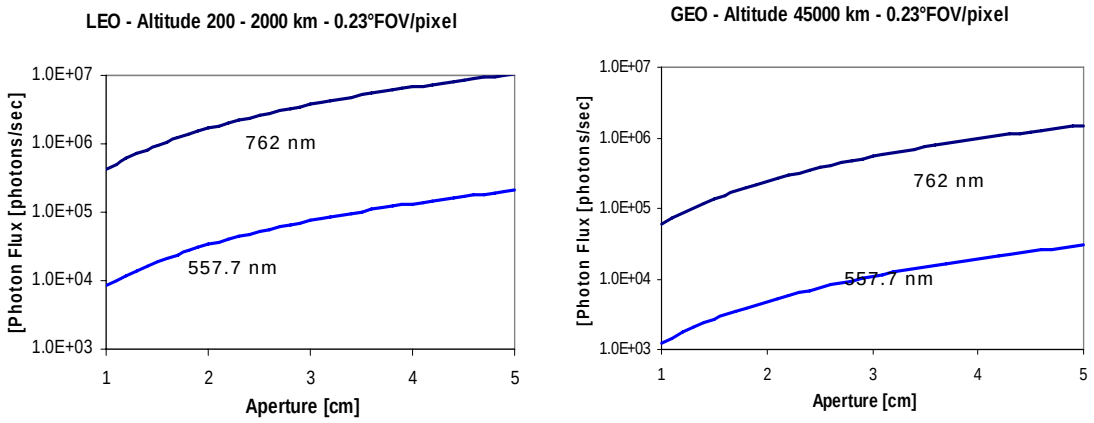

Figure 15: Mean photon flux per pixel at night for different aperture sizes, assuming a FOV of 0.15°/pixel, for LEO (left) and GEO (right).

A good compromise has to be found to guarantee a robust airglow signal. Based on an initial trade-off, our current baseline telescope aperture is 10 mm. Assuming a PDP of 5 %, a FF[1] of 15 % and a Dark Count Rate of 30 Hz, the minimum integration time to guarantee a SNR of 3 for limb measurements of the 762 nm band is 0.05 s for a LEO and 0.50 s for a GEO.

[1] Including the microlenses.

By choosing an appropriate algorithm, the output accuracy for a LEO and a GEO is equal to the half the FOV of one pixel (0.16°). However, errors in the measurements and the calculations will be introduced by:

- the optics aberrations and the correction for distortion (<1 pixel)
- the algorithm used (<1/2 pixels),
- the pointing stability during measurements (smear) (<1/2 pixels)
- the angular incertitude of the airglow (0.2 - 1° for LEO),
- misinterpretation of the measurements due to aurora or the zone near solar terminator,
- the oblateness of the Earth (0.2 – 1° for LEO).

The targeted XY output accuracy is 5° for LEO and 0.6° for GEO. A first baseline design of the Earth Sensor is summarized in Table 4.

Table 4

AIRGLOW OF THE O(^{1}S) GREEN LINE AT 557.7 NM

	Baseline design for a LEO application	Baseline design for a GEO application
Optical system		
Geometry	"triple-tube" design	"single-tube" design
Aperture	10 mm	10 mm
Focal length	14 mm	14 mm
Total FOV	3 x 20°	20°
FOV per pixel	0.16°/pixel	0.16°/pixel
Detector		
Array size	3 x (128 pixels x 128 pixels)	128 pixels x 128 pixels
Pixel size	60 µm x 60 µm	60 µm x 60 µm
Earth Sensor Output		
SNR	≥ 3	≥ 3
Targeted X,Y accuracy 2 σ	5°	0.6°

6. CONCLUSION

We described a novel concept for a low cost Earth Sensors based on imaging atmospheric oxygen emission at 762 nm using arrays of single photon avalanche diodes (SPADs). The use of visible band rather than the LWIR band offers several advantages, including higher sensitivity, lower cost, simpler optics, and a more relaxed thermal design.

The SPADs high sensitivity enables the ES to operate at night and day, over a wide temperature range, with a very compact optical system, with an aperture of 10 mm, focal length of 14 mm, no scanning elements.

In both daytime and night time, there is continuous emission at 762 nm due to atomic oxygen recombination or excitation. Even if the emission at the limbs is 100 times stronger in the day than at night, we show that there is ample unambiguous signal for the operation of an ES using this wavelength if measured with an appropriate detector and an adapted algorithm to determine the Earth vector.

We are currently developing more complete Earth Model as well as optimized SPAD arrays that will be tested for radiation tolerance in order to show the feasibility of the propose ES concept. In parallel a prototype using this ES concept is designed and will be tested in space with the SwissCube satellite.[22]

ACKNOWLEDGEMENTS

We wish to thank Muriel Noca, Prof. Ernest Kopp, Prof. Werner Schmutz, Dr. Jaceck Stegmann and Stephen P. Airey for very helpful discussions and their generous assistance.

The development of the Earth Sensor concept as well as optimized SPAD array are funded by the European Space Agency under contract #20267.

REFERENCES

1. Shuttle Payload Programs: http://glw.lpl.arizona.edu/glo, January 2007
2. C. McDade et al., “ETON 2: Quenching parameters for the proposed precursors of O2(b1∑g+) and O(1S) in the terrestrial nightglow”, *Planet. Space Sci*, 34: p. 789, 1986
3. G.G. Shepherd, Y.-M. Cho, G. Liu, M.G. Shepherd, R.G. Roble, “Airglow variability in the context of the global mesospheric circulation”, *J. atmos. solar-terr. Phys.*, 2006
4. The WINDII Science Page: http://www.windii.yorku.ca/science/science.html, September 2006
5. R.G.H. Greer et al., “ETON 1: A data base pertinent to the study of energy transfer in the oxygen nightglow”, *Planet. Space Sci*, 34: p. 771, 1986
6. Physics of the Aurora : Earth systems, http://meted.ucar.edu/hao/aurora/txt/x_menu.php, September 2006
7. O. Harang, M.J. Kosch, “Absolute optical calibrations using a simple tungsten bulb: theory”, *Sodankylä Geophysical Observatory Publications*, 92:121-123, 2003
8. Rochas, “Single Photon Avalanche Diodes in CMOS Technology”, Ph.D. Thesis, Lausanne, 2003

9. S. Cova, M. Ghioni, A. Lacaita, C. Samori, and F. Zappa, "Avalanche Photodiodes and Quenching Circuits for Single-Photon Detection", *Applied Optics*, Vol. 35. N. 12, Apr. 1996

10. Niclass, A. Rochas, P.A. Besse, E. Charbon, "A CMOS Single Photon Avalanche Diode Array for 3D Imaging", *IEEE International Solid-State Circuits Conference* (ISSCC), pp. 120-121, Feb. 2004

11. C. Niclass, A. Rochas, P.A. Besse, and E. Charbon, "Design and Characterization of A CMOS 3D Image Sensor based on Single Photon Avalanche Diodes", *IEEE Journal of Solid-State Circuits*, Vol. 40, N. 9, pp. 1847-1854, Sep. 2005

12. C. Niclass, M. Sergio, and E. Charbon, "A Single Photon Avalanche Diode Array Fabricated in Deep-Submicron CMOS Technology", *Design and Test in Europe*, Mar. 2006

13. D. Mosconi, D. Stoppa, L. Pacheri, L. Gonzo, A. Simoni, "CMOS Single-Photon Avalanche Diode Array for Time-Resolved Fluorescence Detection", *IEEE ESSCIRC*, Sept. 2006

14. C. Niclass *et al.,* "A 4μs Integration Time Imager Based on CMOS Single Photon Avalanche Diode Technology", *Sensors and Actuators: Physical*, Vol. A130-131, pp. 273-281, Aug. 2006

15. C. Niclass, M. Sergio, and E. Charbon, "A CMOS 64x48 Single Photon Avalanche Diode Array with Event-Driven Readout", *IEEE ESSCIRC*, Oct. 2006

16. C. Niclass, A. Rochas, P.A. Besse, E. Charbon, "Toward a 3-D Camera Based on Single Photon Avalanche Diodes", *IEEE Journal of Selected Topics in Quantum Electronics,* Vol. 10, N.4, Jul./Aug. 2004

17. M. Gersbach, C. Niclass, M. Sergio, D. L. Boiko, C. Petersen, E. Charbon, "Time-Correlated Fluorescence Microscopy Using a Room Temperature Solid-State Single Photon Sensor", *Int. Conference on Near-Field Optics, Nanophotonics and Related Techniques* (NFO), Sep. 2006

18. M. Gösch, *et al.,* "Parallel Single Molecule Detection with Fully Integrated Single Photon 2x2 CMOS Detector Array", *Journal of Biomedical Optics*, Vol. 9, N. 5, pp. 913-921, Spe./Oct. 2004

19. F. Stellari, J. C. Peilin Song Tsang, M.K. McManus, M.B. Ketchen, "Testing and diagnostics of CMOS circuits using light emission from off-state leakage current", *IEEE Trans. on Electron Devices* (IEDM), Vol. 51, N. 9, pp. 1455-1462, Sep. 2004

20. W. Becker *et al*., "Fluorescence lifetime images and correlation spectra obtained by multidimensional time-correlated single photon counting", *Microscopy Research and Technique*, Vol. 69, pp.186-195, 2006

21. M. Sergio, C. Niclass, E. Charbon, "A 128x2 CMOS Single Photon Streak Camera with Timing-Preserving Latchless Pipeline Readout", *IEEE International Solid-State Circuits Conference* (ISSCC), to appear, Feb. 2007

22. Personal communication from Dr. E. Rugi Grond, Oerlikon Space AG, Zurich, Switzerland, January 2007

23. SwissCube satellite experiment: http://swisscube.epfl.ch, January 2007